

ESO Phase 3 Data Release Description

| | |
|------------------------|----------------|
| Data Collection | <i>KiDS</i> |
| Release Number | 1 |
| Data Provider | Konrad Kuijken |
| Date | 30.04.2013 |

Abstract

This data release constitutes the first public release by the Kilo-Degree Survey (KiDS). KiDS is an ESO public survey carried out with the VLT Survey Telescope and OmegaCAM camera, that will image 1500 square degrees in four filters (u, g, r, i), in single epochs per filter. KiDS is designed to be a weak lensing shear tomography survey, and has as its core science drivers mapping of the large-scale matter distribution in the universe and constraining the equation-of-state of Dark Energy. Secondary science cases are manifold and range from galaxy evolution to Milky Way structure, and from detection of white dwarfs to high-redshift quasars.

This first data release encompasses the first 50 square degrees that were observed in all filters. The data were taken under ESO programme IDs: 177.A-3016(A), 177.A-3016(B), 177.A-3016(C), 177.A-3016(D), and 177.A-3017(A). Provided in this release are the calibrated, stacked images and their weights, as well as masks and single-band source lists extracted from the stacks.

Overview of Observations

This data release (KiDS-ESO-DR1) consists of the first 50 “tiles” of KiDS that each were observed in all 4 filters (u,g,r,i), during the first year of regular operations (15 October 2011 to 31 September 2012), and including data taken during Early Science Time (13 August to 15 October 2011). Partial observations for many of the other fields exist as well and will be included in future releases once their wavelength coverage is complete.

Figure 1 shows the locations on the sky of these 50 tiles within the KiDS fields. For each of these tiles, data products based on observations in the bands u, g, r, and i are included.

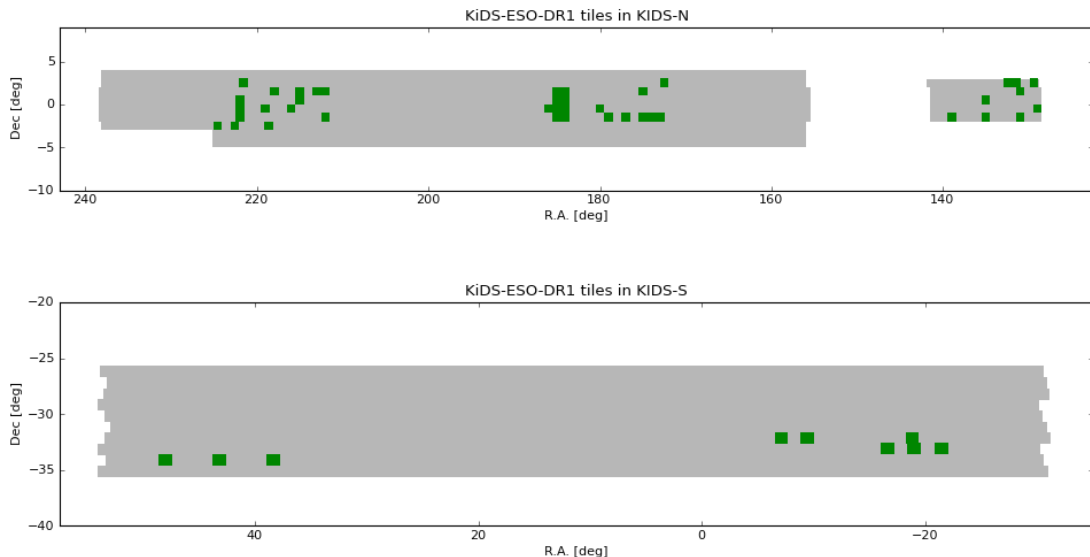


Figure 1: location of the 50 KiDS-ESO-DR1 tiles; the two KiDS fields (top: KiDS-North; bottom: KiDS-South) are outlined in grey, with the tiles included in this data release in green.

Release Content

The complete list of tiles included in KiDS-ESO-DR1 is provided in Table 1, including the tile names (object identifiers) and the coordinates of the tile centers in degrees (J2000.0).

Each tile was observed in u, g, r, and i band. The final footprint of each tile is slightly larger than 1 square degree due to the dithering scheme: 61.9x65.4 arcminutes in u; 62.3x66.8 arcminutes in g, r and i. Taking this into account, the total sky coverage is approximately 55 square degrees, which is not contiguous, as illustrated in Figure 1.

The source lists provided in this data release are single-band and were extracted from the calibrated, stacked images for each tile and filter separately.

| Tile name | RA_J2000 (deg) | DEC_J2000 (deg) | Tile name | RA_J2000 (deg) | DEC_J2000 (deg) |
|-----------------|----------------|-----------------|------------------|----------------|-----------------|
| KIDS_129.0_-0.5 | 129.0 | -0.5 | KIDS_186.0_-0.5 | 186.0 | -0.5 |
| KIDS_129.4_2.5 | 129.3593 | +2.4780 | KIDS_212.0_-1.5 | 212.0 | -1.4890 |
| KIDS_131.0_-1.5 | 131.0 | -1.4890 | KIDS_212.0_1.5 | 212.0 | +1.4890 |
| KIDS_131.0_1.5 | 131.0 | +1.4890 | KIDS_213.0_1.5 | 213.0 | +1.4890 |
| KIDS_131.4_2.5 | 131.3649 | +2.4780 | KIDS_215.0_0.5 | 215.0 | +0.5 |
| KIDS_132.4_2.5 | 132.3677 | +2.4780 | KIDS_215.0_1.5 | 215.0 | +1.4890 |
| KIDS_135.0_-1.5 | 135.0 | -1.4890 | KIDS_216.0_-0.5 | 216.0 | -0.5 |
| KIDS_135.0_0.5 | 135.0 | +0.5 | KIDS_218.0_1.5 | 218.0 | +1.4890 |
| KIDS_139.0_-1.5 | 139.0 | -1.4890 | KIDS_218.6_-2.5 | 218.6072 | -2.4780 |
| KIDS_172.5_2.5 | 172.4791 | 2.4780 | KIDS_219.0_-0.5 | 219.0 | -0.5 |
| KIDS_173.0_-1.5 | 173.0 | -1.4890 | KIDS_221.6_2.5 | 221.6156 | +2.4780 |
| KIDS_174.0_-1.5 | 174.0 | -1.4890 | KIDS_222.0_-0.5 | 222.0 | -0.5 |
| KIDS_175.0_-1.5 | 175.0 | -1.4890 | KIDS_222.0_-1.5 | 222.0 | -1.4890 |
| KIDS_175.0_1.5 | 175.0 | +1.4890 | KIDS_222.0_0.5 | 222.0 | +0.5 |
| KIDS_177.0_-1.5 | 177.0 | -1.4890 | KIDS_222.6_-2.5 | 222.6184 | -2.4780 |
| KIDS_179.0_-1.5 | 179.0 | -1.4890 | KIDS_224.6_-2.5 | 224.6240 | -2.4780 |
| KIDS_180.0_-0.5 | 180.0 | -0.5 | KIDS_338.6_-33.1 | 338.6139 | -33.1374 |
| KIDS_184.0_-0.5 | 184.0 | -0.5 | KIDS_341.0_-33.1 | 340.9901 | -33.1374 |
| KIDS_184.0_-1.5 | 184.0 | -1.4890 | KIDS_341.2_-32.1 | 341.1765 | -32.1484 |
| KIDS_184.0_0.5 | 184.0 | +0.5 | KIDS_343.4_-33.1 | 343.3663 | -33.1374 |
| KIDS_184.0_1.5 | 184.0 | +1.4890 | KIDS_350.6_-32.1 | 350.5882 | -32.1484 |
| KIDS_185.0_-0.5 | 185.0 | -0.5 | KIDS_352.9_-32.1 | 352.9412 | -32.1484 |
| KIDS_185.0_-1.5 | 185.0 | -1.4890 | KIDS_38.4_-34.1 | 38.4 | -34.1264 |
| KIDS_185.0_0.5 | 185.0 | +0.5 | KIDS_43.2_-34.1 | 43.2 | -34.1264 |
| KIDS_185.0_1.5 | 185.0 | +1.4890 | KIDS_48.0_-34.1 | 48.0 | -34.1264 |

Table 1: tile names (object identifiers) and coordinates of the 50 tiles included in KiDS-ESO-DR1.

Since the OmegaCAM CCD mosaic consists of 32 individual CCDs, the sky covered by a single exposure is not contiguous but contains gaps. In order to fill in these gaps, KiDS tiles are built up from 5 dithered observations in g, r and i and 4 in u. The dithers form a staircase pattern with dither steps of 25'' in X (RA) and 85'' in Y (DEC), bridging the inter-CCD gaps (de Jong et al., 2013, ExA 35, 25). The tile centers are based on a tiling strategy that tiles the full sky efficiently for VST/OmegaCAM. Neighbouring dithered stacks have an overlap in RA of 5% and in DEC of 10%.

Exposure times and observing constraints for the four filters are tabulated in Table 2.

| Filter | Max. FLI | Min. moon distance | Max. seeing (arcsec) | Max. airmass | Sky transp. | Dithers | Total Exp. time (s) |
|--------|----------|--------------------|----------------------|--------------|-------------|---------|---------------------|
| u | 0.4 | 90 | 1.1 | 1.2 | CLEAR | 4 | 1000 |
| g | 0.4 | 80 | 0.9 | 1.6 | CLEAR | 5 | 900 |
| r | 0.4 | 60 | 0.8 | 1.3 | CLEAR | 5 | 1800 |
| i | 1.0 | 60 | 1.1 | 2.0 | CLEAR | 5 | 1080 |

Table 2: KiDS observing strategy; observing condition constraints, exposure times, and number of dithers for each filter.

In Figure 2 the obtained seeing (FWHM), PSF ellipticity, and limiting magnitude (5σ AB in $2''$ aperture) distributions per filter are shown, to illustrate the obtained data quality. In case of the filters observed in dark time (u, g, r) the FWHM distributions reflect the different observing constraints, with r-band taking the best conditions. Since i-band is the only filter observed in bright time, it is observed under a large range of seeing conditions. Average PSF ellipticities are always small: <0.1 (the average is over the absolute amount of ellipticity, regardless of the direction of ellipticity). The wide range of limiting magnitudes in i-band is caused by the large range in moon phase and thus sky brightness.

For a full overview of the data quality parameters for each observation we refer to the following online table: http://kids.strw.leidenuniv.nl/DR1/data_table.php

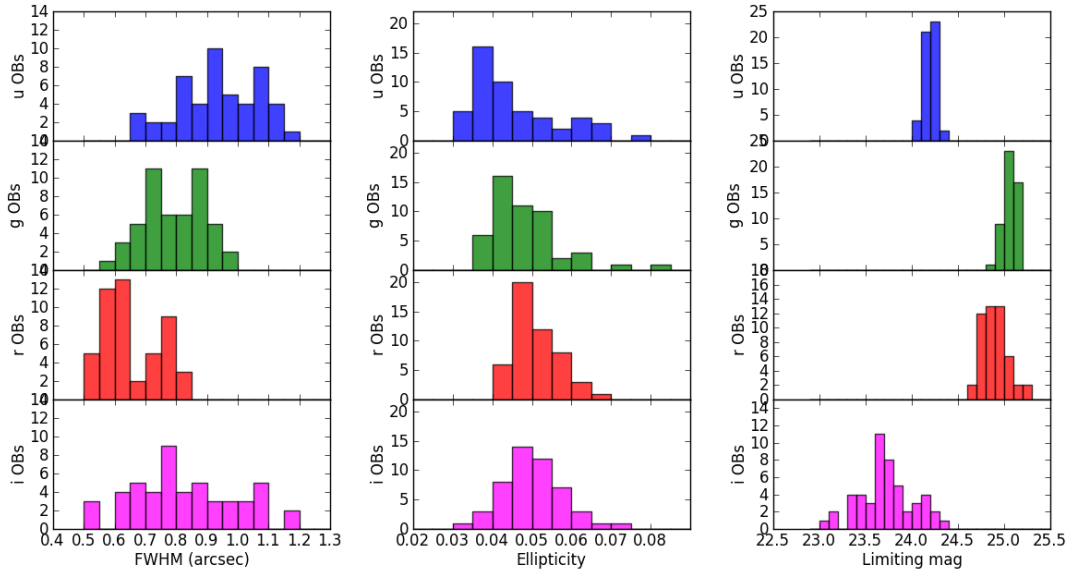


Figure 2: obtained raw data quality parameters for KiDS-ESO-DR1. **Left:** average PSF size (FWHM) distributions; **center:** average ellipticity distributions; **right:** limiting magnitude distributions (5σ AB in $2''$ aperture). The distributions are per filter: from top to bottom u, g, r, and i, respectively.

A total of 800 files is included in this data release: per tile for each filter a stacked image (coadd), a corresponding weight frame, a mask FLAG image, and a source list. The total data volume of this data release is 702 GB.

Release Notes

Data Reduction and Calibration

The KiDS-ESO-DR1 pipeline is based on the Astro-WISE optical pipeline described in McFarland et al. (2013, ExA 35, 79) (MF13). Below we summarize the processing steps and list KiDS-specific information (i.e., KiDS process configuration and departures from Astro-WISE optical pipeline).

Image detrending

Detrending of the raw data consists of the following steps.

- **Cross-talk correction.** Electronic cross-talk occurs between CCDs #93, #94, #95 and #96, resulting in faint imprints of bright sources on neighbouring CCDs. A correction was made for cross-talk between CCDs #95 and #96, where it is strongest (up to 0.7%).
- **De-biasing and overscan correction.** First, for each science and calibration exposure the overscan is subtracted per row (using method 6, see MF13). Second, a daily overscan-subtracted bias is subtracted. This is a daily average of 10 biases with 3σ -rejection.
- **Flat-fielding.** A single masterflat (per CCD and filter) was used for all data in the release. This is by virtue that the intrinsic pixel sensitivities can be considered constant to $\sim 0.2\%$ or better for g, r and i (Verdoes Kleijn et al., 2013, ExA, 35, 103). For g, r and i this master flat is a combination of a master dome (for high spatial frequencies) and master twilight (=sky) flat-field (for low spatial frequencies). Both contributing flats are an average of 5 raw flat-field exposures with 3σ -rejection. In u band only the twilight flats are used.
- **Illumination correction.** Illumination correction (a.k.a. “photometric superflat”) is applied *in pixel space*, and only on the source fluxes (i.e., after background subtraction). A single illumination correction image is used to correct the single master flats per filter for all KiDS-ESO-DR1 data (see Verdoes Kleijn et al., 2013, ExA 35, 103).
- **De-fringing.** De-fringing is only needed for KiDS i-band. Analysis of nightly fringe frames showed that the pattern is constant in time. Therefore, a single fringe image was used for all KiDS-ESO-DR1 images observed after 2012-01-11. For each science exposure this fringe image is scaled (after background subtraction of the science exposure and fringe frame) and then subtracted to minimize residual fringes.
- **Pixel masking.** Cosmic-rays, hot and cold pixels, saturated pixels are automatically masked as described in MF13 during de-trending. These are included in the weight image. Additional automatic and manual masking is applied on the coadds (see below).
- **Satellite track removal.** Satellite tracks are detected automatically by applying the Hough transform (Hough, 1962) to a difference image of maximally overlapping exposures within a dither sequence after masking bright stars and bright ghosts. The pixels affected by satellite tracks are masked and included in the weight image.
- **Background subtraction.** To remove vignetting by bond wire baffling (Iwert et al. 2006, Proc. SPIE 6276, 62760A) in the focal plane, a row-by-row background subtraction method is used, before the background subtraction done by SWARP (see below).

Photometric calibration

The steps taken to calibrate the photometry are as follows.

- KiDS-ESO-DR1 photometric calibration starts with individual zero points per CCD based on SA field observations. The calibration deploys a fixed aperture (6.3 arcsec diameter) not corrected for flux losses, and uses SDSS DR8 PSF magnitudes of stars in the SA fields as reference. Magnitudes are expressed in AB in the instrumental photometric system (i.e., no color corrections between OmegaCAM and SDSS photometric system applied).
- Next, the photometry is homogenized across CCDs and dithers for each filter in each tile independently. This global photometric solution is derived and applied in three steps:
 1. From the overlapping sources across dithered exposures, zero point differences

between the dithers (e.g. due to varying atmospheric extinction) are derived.

2. Zero point differences across CCDs are calculated using all CCD overlaps between the dithered exposures. Steps 1 and 2 both apply a minimization algorithm (see Maddox et al. 1990, MNRAS, 246, 433).
3. The zero point offsets are applied to all CCDs w.r.t. an average zero point valid for the night, derived from the nightly SA field observations. If no SA field observations are available for the night, default values are used instead.

Color terms

The photometric calibration provided in KiDS-ESO-DR1 is in AB magnitudes in the instrumental system. Color-terms have been calculated with respect to the SDSS photometric system.

Aperture magnitudes of point sources were obtained from KiDS observations for apertures with a radius equal to the median FWHM in the observation, using spatially varying aperture corrections. These aperture magnitudes were matched to SDSS (DR8) PSF magnitudes of point-like sources. For each filter, the median offset to SDSS is first subtracted, rejecting tiles where this offset exceeds 0.1 mag in any of the g, r and i bands. The fit is done on all points from the remaining complete tiles (note: not only tiles included in KiDS-ESO-DR1 were used for this analysis). This gives the following results:

$$\begin{aligned} u_{\text{KiDS}} - u_{\text{SDSS}} &= (-0.057 \pm 0.009)(u_{\text{SDSS}} - g_{\text{SDSS}}), \\ g_{\text{KiDS}} - g_{\text{SDSS}} &= (-0.052 \pm 0.003)(g_{\text{SDSS}} - r_{\text{SDSS}}), \\ r_{\text{KiDS}} - r_{\text{SDSS}} &= (-0.032 \pm 0.007)(g_{\text{SDSS}} - r_{\text{SDSS}}), \\ i_{\text{KiDS}} - i_{\text{SDSS}} &= (+0.015 \pm 0.006)(r_{\text{SDSS}} - i_{\text{SDSS}}). \end{aligned}$$

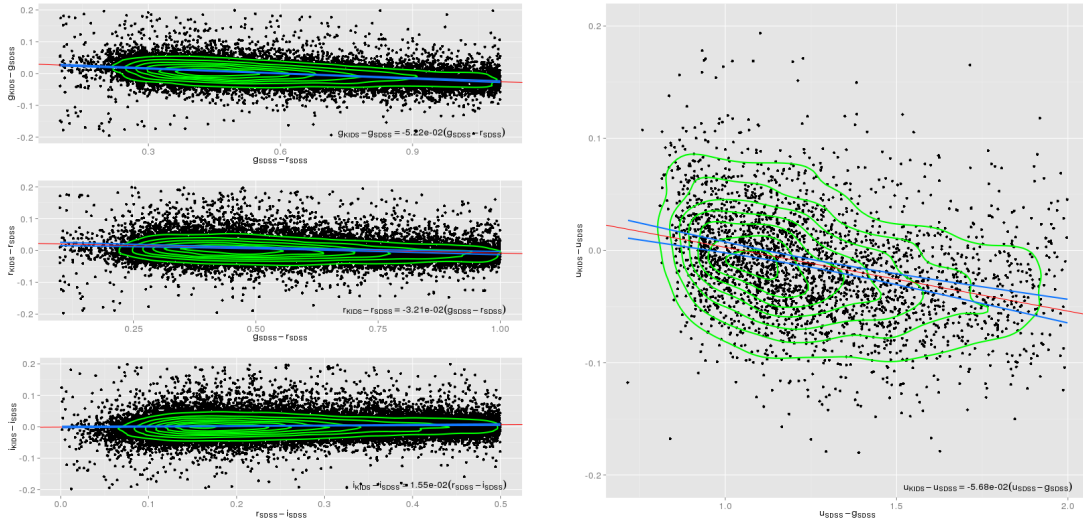


Figure 3: Derivation of color-terms of KiDS photometry w.r.t. the SDSS photometric system. **Left:** from top to bottom: $g_{\text{KiDS}} - g_{\text{SDSS}}$ vs $g_{\text{SDSS}} - r_{\text{SDSS}}$; $r_{\text{KiDS}} - r_{\text{SDSS}}$ vs $g_{\text{SDSS}} - r_{\text{SDSS}}$; $i_{\text{KiDS}} - i_{\text{SDSS}}$ vs $r_{\text{SDSS}} - i_{\text{SDSS}}$. The distribution of stars (black dots) is overlaid with contours (green) and fit by a linear relation (red line, with blue lines indicating the statistical uncertainty). **Right:** similar analysis for $u_{\text{KiDS}} - u_{\text{SDSS}}$ vs $u_{\text{SDSS}} - g_{\text{SDSS}}$.

Astrometry, regridding and coadding

A global (multi-CCD and multi-dither) astrometric calibration is calculated per filter per tile. SCAMP (Bertin 2006, ASP Conf. Series 351, 112) is used for this purpose, with a polynomial degree of 2 over the whole mosaic. The (unfiltered) 2MASS-PSC (Skrutskie et al. 2006, AJ, 131, 1163) is used as astrometric reference catalog. A more detailed description of the astrometric pipeline is in MF13.

SWARP is used to resample all exposures in a tile to the same pixel grid, with a pixel size of 0.2 arcseconds. After background subtraction the exposures are coadded using a weighted mean stacking procedure.

Masking of bright stars and defects

A stand-alone program dubbed Pulecenella v1.0 (Huang et al. 2013, in prep.) was developed to create masks for KiDS-ESO-DR1 coadds. It is an automatized procedure for mask creation completely independent from external star catalogs. An example of a detail of a mask is shown in Figure 4. Pulecenella detects the following types of critical areas, all related to bright stars:

- saturated pixels,
- spikes caused by diffraction by the mirror supports,
- readout spikes,
- reflection halos produced by the optics components (a central core halo, and up to three wider reflection halos with spatially dependent offsets, depending on the brightness of the star).

Defects that are not related to bright stars, such as satellite tracks (if missed by automated masking during de-trending) or other artifacts, are not detected by Pulecenella; for KiDS-ESO-DR1 coadds these areas have been masked by hand and included in the final masks.

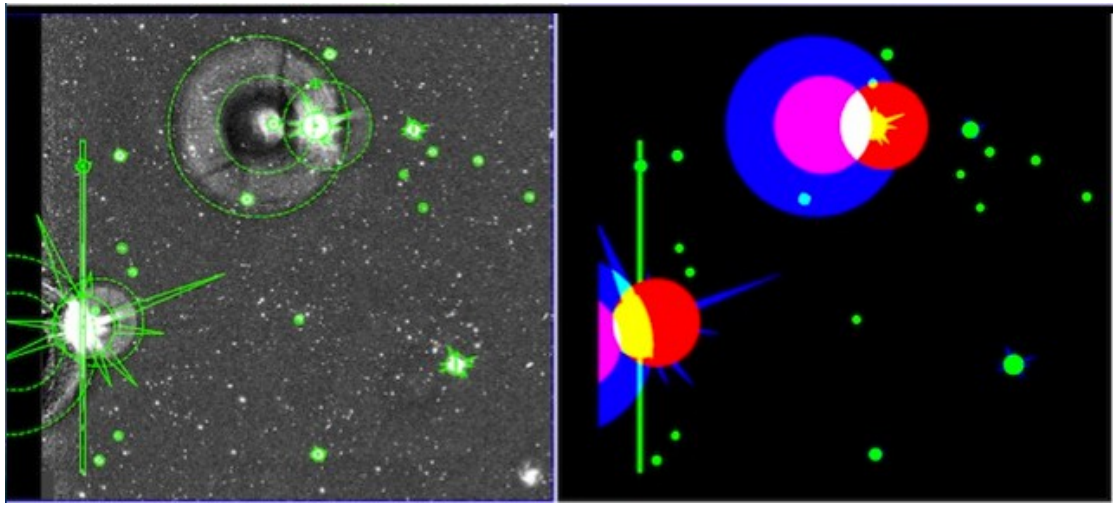


Figure 4: Detail of a Pulecenella v1.0 mask. **Left:** detail of a KiDS stacked image with bright stars; critical areas detected by Pulecenella are overplotted with green outlines. **Right:** FLAG image corresponding to the image shown on the left, with different colors indicating the pixel values resulting from the combination of different flag values.

The masks are provided as FITS FLAG images, where each type of critical region is identified by a different flag value, as listed in Table 3. During source extraction for the single-band source list (see below) the FLAG image is used to flag sources whose isophotes overlap with the critical areas. The resulting flags are stored in the following two source parameters:

- IMAFLAGS_ISO: FLAG image flags OR'd over the isophote profile
- NIMAFLAG_ISO: number of flagged pixels entering IMAFLAGS_ISO

| Type of area | Flag value | Type of area | Flag value |
|-------------------|------------|------------------------|------------|
| Readout spike | 1 | Secondary halo | 16 |
| Saturation core | 2 | Tertiary halo | 32 |
| Diffraction spike | 4 | Bad pixel | 64 |
| Primary halo | 8 | Manually masked region | 128 |

Table 3: Critical areas in the masks and their flag values.

Source list extraction and star/galaxy separation

The source lists delivered in this data release are intended as “general purpose” source lists. Source list extraction and star/galaxy (hereafter S/G) separation is done with an automated stand-alone procedure optimized for KiDS data: KiDS-CAT. This procedure, the backbone of which is formed by S-Extractor (Bertin & Arnouts, 1996, A&AS, 317, 393) performs the following steps.

1. S-Extractor is run on the stacked image to measure the FWHM of all sources. High-confidence star candidates are then identified (for details see La Barbera et al. 2008, PASP, 120, L681).
2. The average PSF FWHM is calculated by applying the bi-weight location estimator to the FWHM distribution of the high-confidence star candidates.
3. A second pass of S-Extractor is done with SEEING_FWHM set to the derived average PSF FWHM. During this second pass the image is background-subtracted, filtered and thresholded “on-the fly”. Detected sources are then de-blended, cleaned, photometered, and classified. A number of S-Extractor input parameters are set individually for each image (e.g., SEEING_FWHM and GAIN), while others have been optimized to provide the best compromise between completeness and spurious detections (see Data Quality section below). The detection set-up used is summarized in Table 4; a full S-Extractor config file is available at this URL:
http://kids.strw.leidenuniv.nl/DR1/example_config.sex
Apart from isophotal magnitudes and Kron-like elliptical aperture magnitudes, a large number of aperture fluxes are included in the source lists. This allows users to estimate aperture corrections and total source magnitudes. All parameters provided in the source lists are listed in the Data Format section below.
4. S/G separation is performed based the CLASS_STAR (star classification) and SNR (signal-to-noise ratio) parameters provided by S-Extractor and consists of the following steps:
 - In the SNR range where the high-confidence star candidates are located (the red dots in Figure 5) the bi-weight estimator is used to define their CLASS_STAR location, θ , and its width, σ ; a lower envelope of $\theta - 4\sigma$ is defined.
 - At SNR below that of the high-confidence star candidates, a running median CLASS_STAR value is computed from sources with CLASS_STAR > 0.8, which is shifted to match the $\theta - 4\sigma$ locus. The resulting curve (blue curve in Figure 5) defines the separation of stars and galaxies.

The source magnitudes and fluxes in the final source lists are not corrected for Galactic foreground or intergalactic extinction. The result of the S/G classification is available in the source lists via the 2DPHOT flag. Flag values are: 1 (high-confidence star candidates), 2 (objects with FWHM smaller than stars in the stellar locus, e.g., some cosmic-rays and/or other unreliable sources), 4 (stars according to S/G separation), and 0 otherwise (galaxies); flag values are summed, so 2DPHOT = 5 signifies a high-confidence star candidate that is also above the S/G separation line.

Additional information, and source lists with alternative detection set-ups can be found on the following website: <http://kids.strw.leidenuniv.nl/DR1/>

| Parameter | Value | Description |
|-----------------|--------------|--|
| DETECT_THRESH | 1.5 | <sigmas> or <threshold>,<ZP> in mag.arcsec ⁻² |
| DETECT_MINAREA | 3 | minimum number of pixels above threshold |
| ANALYSIS_THRESH | 1.5 | <sigmas> or <threshold>,<ZP> in mag.arcsec ⁻² |
| DEBLEND_NTHRESH | 32 | Number of deblending sub-thresholds |
| DEBLEND_MINCONT | 0.001 | Minimum contrast parameter for deblending |
| FILTER | Y | Apply filter for detection (Y or N) |
| FILTER_NAME | default.conv | Name of the file containing the filter |
| CLEAN | Y | Clean spurious detections? (Y or N)? |
| CLEAN_PARAM | 1.0 | Cleaning efficiency |
| BACK_SIZE | 256 | Background mesh: <size> or <width>,<height> |
| BACK_FILTERSIZE | 3 | Background filter: <size> or <width>,<height> |
| BACKPHOTO_TYPE | LOCAL | can be "GLOBAL" or "LOCAL" |
| BACKPHOTO_THICK | 24 | thickness of the background LOCAL annulus |

Table 4: detection set-up for KiDS-ESO-DR1 single-band source lists

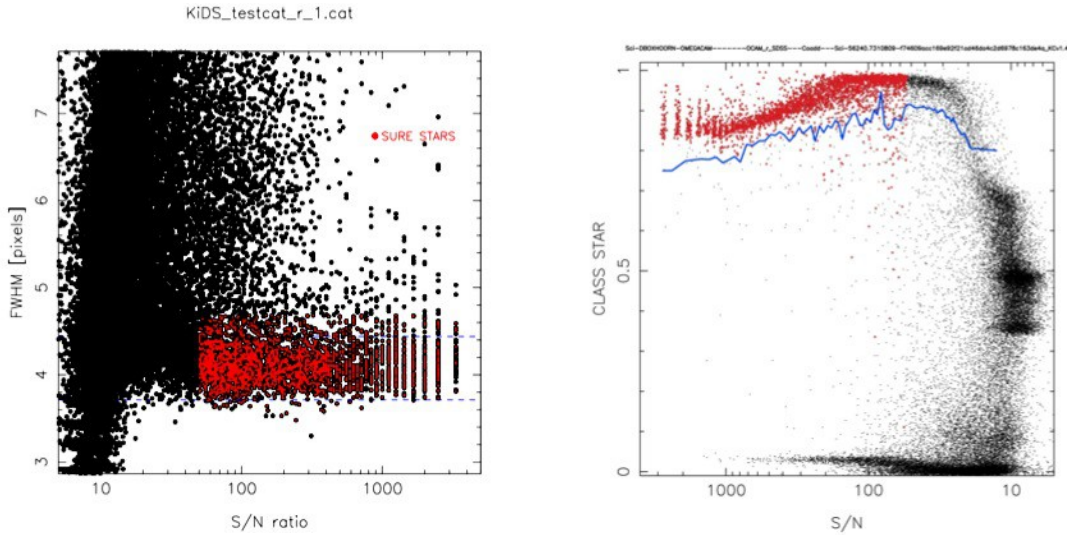


Figure 5: High-confidence star candidates and star/galaxy separation. **Left:** the high-confidence star candidates (red dots) are used to locate the stellar locus and calculate the average FWHM of the image. **Right:** example of star/galaxy separation; at SNR >50, the high-confidence star candidates (red dots) are used to define the blue line; at lower SNR, all sources with CLASS_STAR >0.8 are used; sources above the blue line are classified as stars.

Data Quality

Photometric quality

The matter of photometric quality can be split up in two:

1. the uniformity of the photometry within each tile
2. the quality of the absolute photometric calibration per tile/filter

Unfortunately, the distribution of tiles included in KiDS-ESO-DR1 is not contiguous, with many isolated tiles. Because of this, a complete homogenization of the photometric calibration for the entire data set was not possible. This should improve greatly in future releases.

Both the internal photometric homogeneity within a coadd and the quality of the absolute photometric scale is assessed by comparing the KiDS-ESO-DR1 photometry to SDSS DR8 (Aihara et al., 2011, ApJS, 193, 29). This comparison can be done for all 41 tiles in the KiDS-North field (Fig. 1). KiDS-South was calibrated in the same way as KiDS-North, so we expect the conclusions to hold for these data as well.

PSF magnitudes were extracted from SDSS DR8 and compared to KiDS total magnitudes based on aperture magnitudes within an aperture of 2 times the FWHM applying a spatially dependent aperture correction derived from 10 arcsec aperture photometry of bright, non-saturated stars.

Figure 6 shows the offsets between KiDS-ESO-DR1 and SDSS DR8 magnitudes for 1 tile (KIDS_173.0_-1.5), which is a representative example. Generally the photometry in one filter is uniform to within a few percent. Average peak-to-valley variations within a coadd are listed per filter in Table 5.

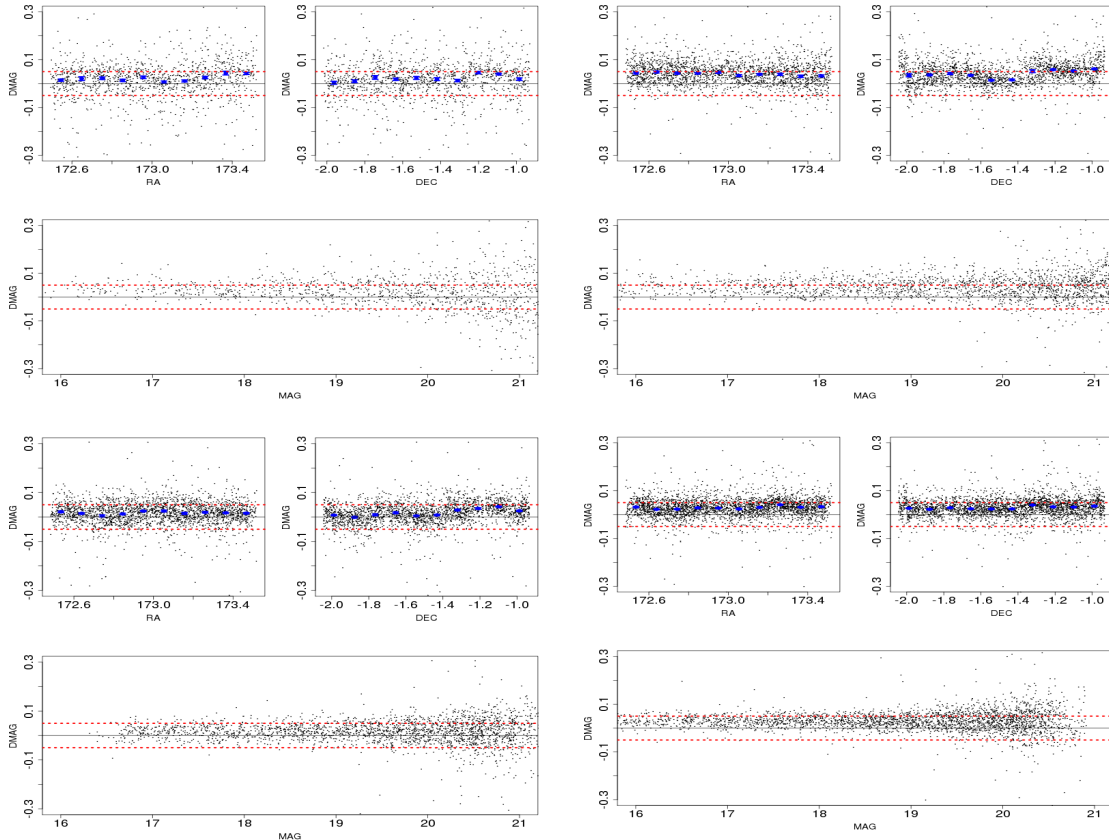


Figure 6: KiDS – SDSS DR8 magnitude offsets for stars in tile KiDS 173.0 -1.5 for *u* (top left), *g* (top right), *r* (bottom left) and *i* (bottom right). For each filter residual magnitudes are plotted as a function of RA, DEC (top row) and magnitude (bottom panel). Each dot corresponds to a star, while running medians are shown as blue bars. The red dotted lines indicate $+0.05$ and -0.05 magnitudes.

| Coadd photometric homogeneity | |
|-------------------------------|---|
| Filter | $\Delta\text{mag}_{\text{max}} - \Delta\text{mag}_{\text{min}}$ (mmag) |
| u | ~36 |
| g | ~32 |
| r | ~25 |
| i | ~21 |

Table 5: Amplitudes of the variation in the photometric offset between KiDS and SDSS DR8 across coadds in KiDS-ESO-DR1.

The quality of the absolute photometric scale is illustrated in Fig. 7, where the photometry is compared between KiDS and SDSS for the 41 tiles in the overlapping area. A systematic offset of ~ 0.02 mag is present in g, r, and i. This could be due to the fact that nightly zero points are determined using a fixed aperture on stars in the SA field without aperture correction. The scatter apparent in Fig. 7 is probably due to non-photometric conditions (during either KiDS or SA field observations) and use of default zero points for nights without good SA observations. Corrections for both become possible in future releases with significant contiguous area, which will allow a global calibration for the entire survey.

Astrometric quality

The accuracy of the absolute astrometry (“KiDS vs 2MASS”) is uniform over a coadd, with typical 2-dimensional RMS of 0.31 arcsec in g, r, and i, and 0.25 arcsec in u (Fig. 8). The lower RMS in u-band is most likely due to the fact that in this band on average brighter 2MASS sources are selected as reference sources.

The accuracy of the relative astrometry (“KiDS vs KiDS”) is also uniform across a single coadd. This is indicated by the 2-dimensional positional residuals of sources across its input dithers (Fig. 10). The residuals have a RMS of ~ 0.029 arcsec for g, r and i and ~ 0.032 arcsec for u. The slightly larger RMS in u-band is due to the smaller number of available reference sources. In Figure 7 the accuracy of the relative astrometry of all coadds is shown. Overall, the RMS is ~ 0.030 arcsec for g, r and i. For u the scatter is larger with maximum rms ~ 0.055 arcsec.

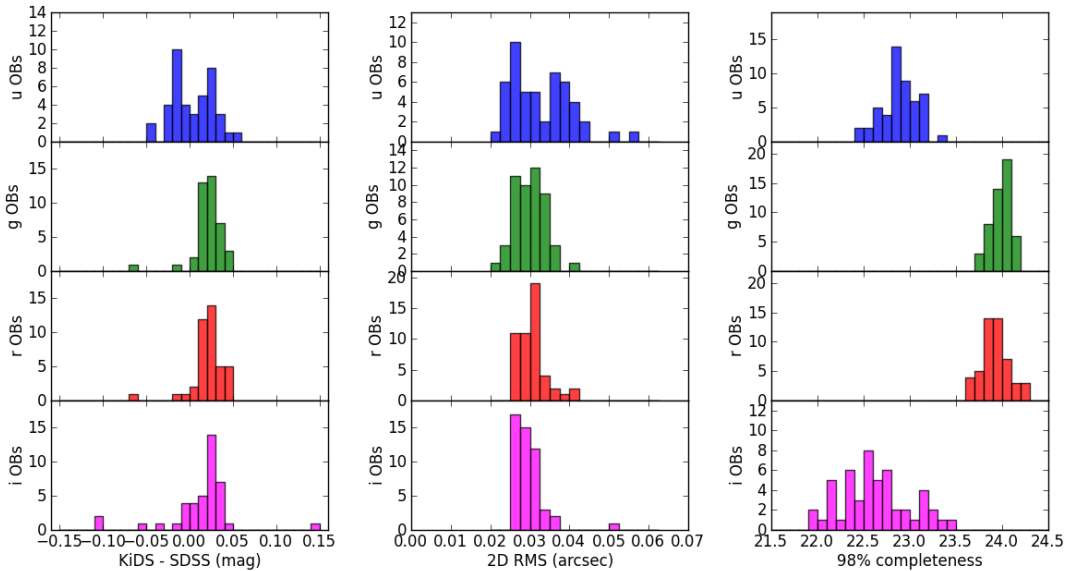


Figure 7: Photometric, astrometric and completeness overview of KiDS-ESO-DR1. **Left:** median photometric offsets for stars between the 41 tiles in KiDS-North and SDSS DR8. **Center:** median relative astrometric offsets between the dithers in a coadd. **Right:** 98% completeness magnitude distributions for all tiles included in KiDS-ESO-DR1. In all columns the panels correspond to u, g, r, and i from top to bottom.

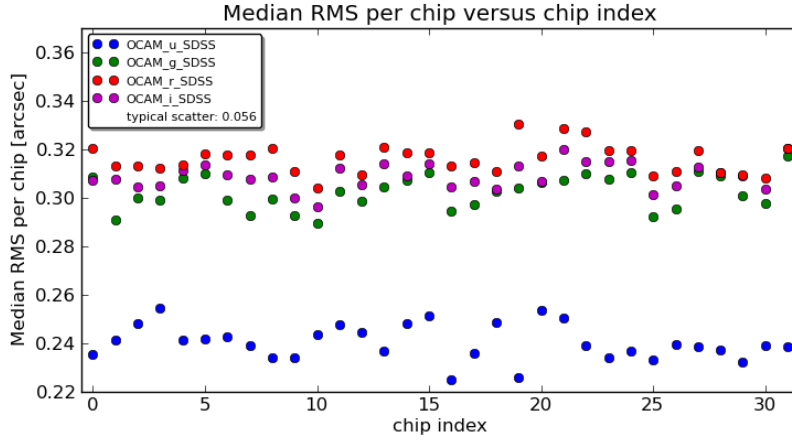


Figure 8: Absolute astrometric accuracy across a KiDS coadd, based on the RMS of the 2-dim. positional residual of KiDS – 2MASS source pairings across dithers. Plotted is the median of the RMS ensemble of all 50 KiDS tiles per CCD (chip) for u (blue), g (green), r (red) and i (magenta). The typical standard deviation in this RMS ensemble is 0.056 arcsec and is similar for all CCDs and filters.

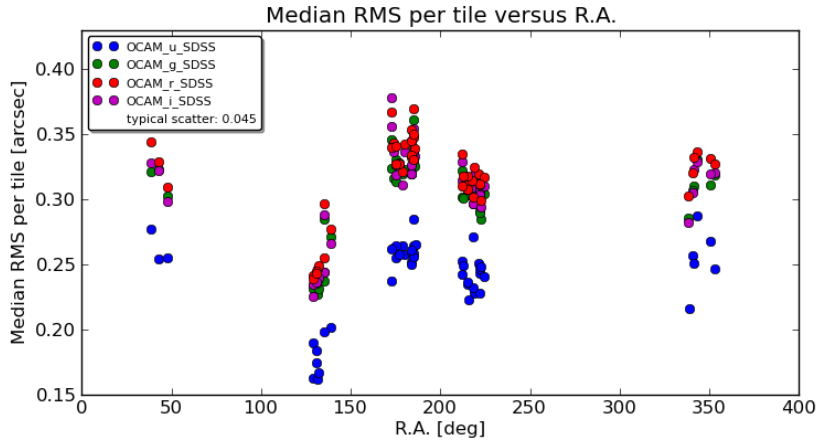


Figure 9: Absolute astrometric accuracy versus RA, based on the RMS of the 2-dim. positional residual of source pairings across dithers as in Fig. 8. Plotted is the median RMS for each coadd with colors indicating the filter: u (blue), g (green), r (red) and i (magenta).

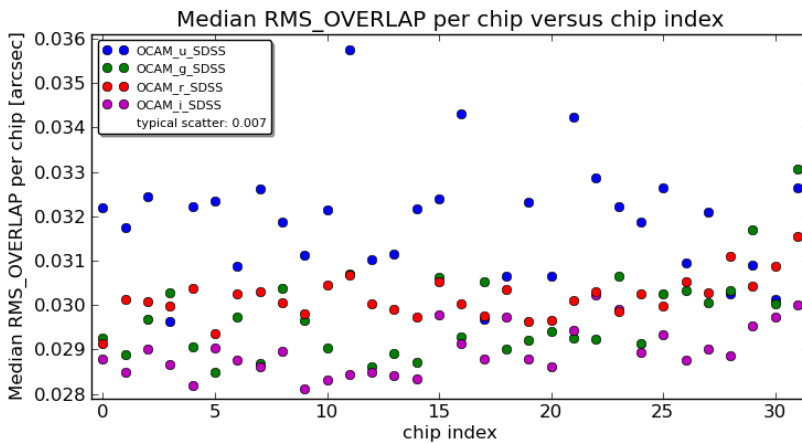


Figure 10: Relative astrometric accuracy across a KiDS coadd. It uses the RMS of the 2-dim. positional residual of source pairings across dithers versus chip index. Plotted is the median of the RMS ensemble of all 50 KiDS tiles for u, g, r and i. The typical standard deviation in this ensemble is 0.007 arcsec and is similar for all chips and filters.

Completeness and contamination

The contamination of the KiDS-ESO-DR1 source lists for unflagged sources is estimated to be $<4\%$ down to a $\text{SNR} \sim 5$ within a 2 arcsec aperture (see Fig. 11). Ignoring all source extraction flags and masking, the corresponding spurious fraction increases to at most 10%. At very low SNR ($\lesssim 3$), the spurious fraction increases dramatically, and we advise users of the source lists to filter out all sources below a SNR threshold of 3.0.

The spurious fractions are determined through a comparison to the r-band data of the CFHT Legacy Survey (<http://www.cfht.hawaii.edu/Science/CFHLS/>), the main deeper survey overlapping with the current release (CFHTLS-W2, using their final data release T0007). For the analysis it is assumed that all KiDS sources not detected in CFHTLS-W2 are spurious. These values come with a caveat: they were only determined accurately in r-band and for a small area ($< 1 \text{ sq.deg.}$).

An internal estimate of the completeness for KiDS-ESO-DR1 source lists is provided, based on the method of Garilli et al. 1999 (A&A, 342, 408). It determines the magnitude at which objects start to be lost in the source list because they are below the brightness threshold in the detection cell. The implementation is similar to La Barbera et al. (2010, MNRAS, 408, 1313). Estimates of the completeness obtained by comparison to deeper CFHTLS-W2 data are consistent with these internally derived values. The distributions of the 98% completeness magnitudes for all tiles are shown in Fig. 7. Comparison with Fig. 2 shows that the 98% completeness limits are typically ~ 1 magnitude brighter than the limiting magnitude for g, r and i and ~ 1.3 magnitudes brighter in u.

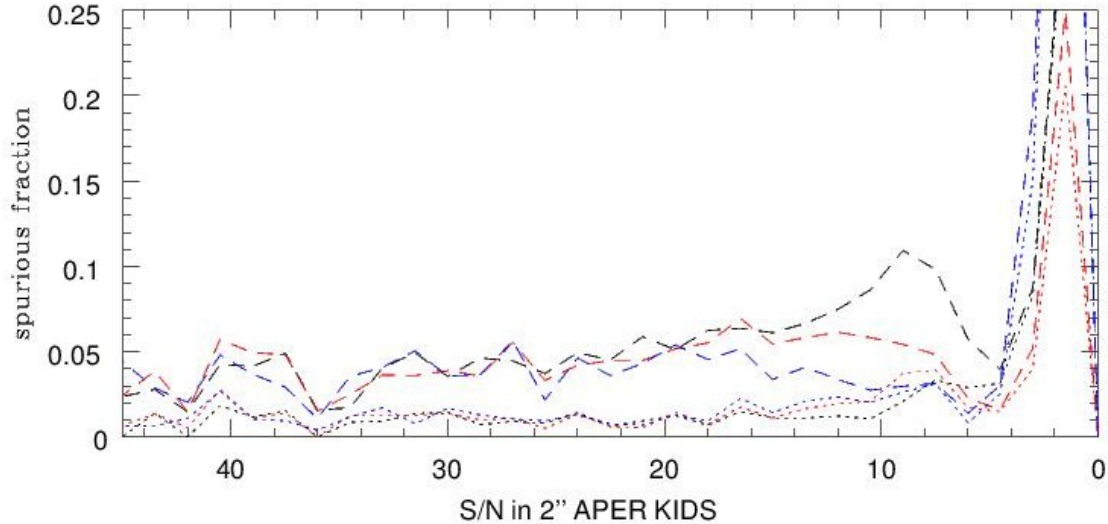


Figure 11: Spurious fraction in the r-band image of KiDS 135.0 -1.5 as a function of S/N in a 2 arcsec aperture. Dotted lines correspond to sources without flags, dashed lines to all sources. The colors differentiate between using a S-Extractor configuration with $\text{DETECT_THRESH}=2.5$ (blue), 2.0 (red), 1.5 (black) respectively. For this KiDS-ESO-DR1 release a $\text{DETECT_THRESH}=1.5$ is applied.

Known issues

Scattered light and reflections

Some of the main issues in the early VST/OmegaCAM data are related to scattered light and reflections. Due to the open structure of the telescope, light from sources outside the field-of-view is often affecting the observations. This expresses itself in a number of ways:

- reflections: in some cases strong reflected light patterns are seen in the focal plane; these are caused by light from bright point sources outside the field-of-view and can occur in all filters. Some examples are shown in Fig. 12a.
- vignetting by CCD masks: vignetting and scattering by the masks present at the corners of the focal plane array, and at the gaps between the rows of CCDs; this effect is particularly strong in i-band due to the bright conditions. The effect near the CCD gaps is largely corrected for, but in many cases the areas in the corners of the CCD array is strongly affected. Examples are shown in Fig. 12b.
- extended background artifacts: related to the reflections mentioned before, this is mostly seen in i-band and probably caused by moonlight. An example is shown in Fig. 12c.

Most of these effects are not (yet) corrected for in the current data processing, but strongly affected regions are included in the image masks provided in this data release and affected sources are flagged in the source lists.

Improvements to the telescope baffles that should significantly improve scattered light suppression are being considered by ESO.

Individual CCD issues

There are two issues related to individual CCDs that noticeably affect this data delivery:

- CCD 82: this CCD suffered from random gain jumps and related artifacts until its video board was replaced on June 2 2012. Artefacts as shown in Fig. 12d are sometimes visible in the image stacks due to this problem. Photometry in this CCD can be used due to the cross-calibration with neighbouring CCDs in the dithered exposures, but part of the CCD is lost. These features are included in the image masks and affected sources are flagged.
- CCD 93: during a few nights in September 2011 (Early Science Time) one CCD was effectively dead due to a video cable problem. One observation included in this data delivery does not include this CCD: the i-band observation of KIDS_341.2_-32.1.

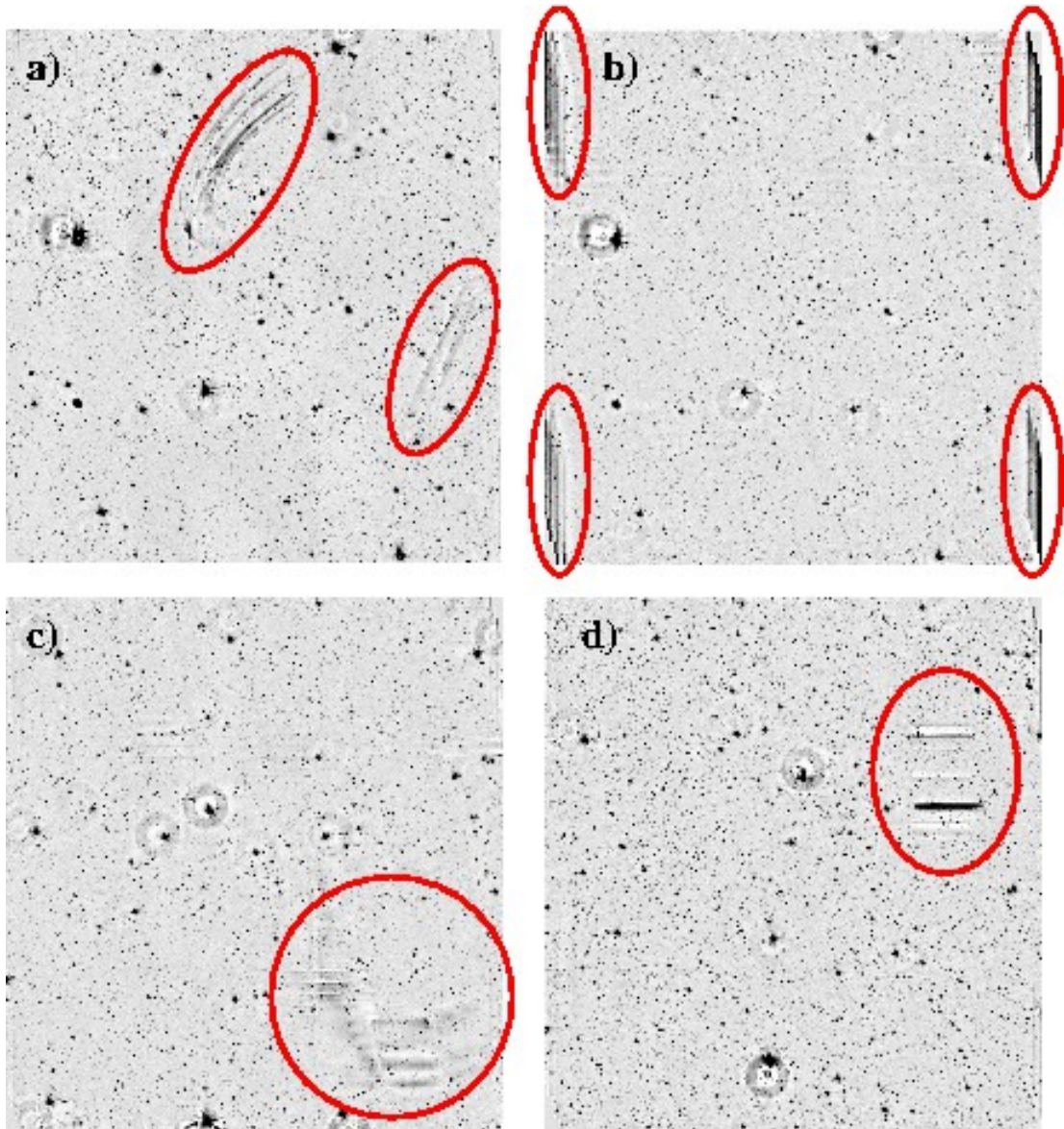


*Figure 12: examples known issues in the VST/OmegaCAM data, highlighted by the red ellipses. **a)** light patterns caused by reflections and scattered light of bright sources outside the FOV. **b)** vignetting and scattering by CCD masks at the corners of the CCD array. **c)** extended background structures caused by scattering of moonlight. **d)** patterns caused by defective video board of CCD 82.*

Data Format

File Types

Table 6 lists the types of data products provided in this release, together with descriptions of the file types and naming conventions used.

The naming convention used for all data products is the following:

`KiDS_DR1.0_R.R_D.D_F_TTT.fits`,

where R.R and D.D are the RA and DEC of the tile center in degrees (J2000.0) with 1 decimal place, F is the filter (u, g, r, or i), and TTT is the data product type. The value of TTT for the different data products is given in column 4 of Table 6.

For example: the r-band stacked image of the tile “KIDS_48.3-33.1” is called

`KiDS_DR1.0_48.3_-33.1_r_sci.fits`.

| Data product | ESO product category name | File type | TTT |
|----------------------------|---------------------------|-------------------|-----|
| Calibrated, stacked images | SCIENCE.IMAGE | FITS image | sci |
| Weight frames | ANCILLARY.WEIGHTMAP | FITS image | wei |
| Masks | ANCILLARY.MASK | FITS image | msk |
| Single-band source lists | SCIENCE.SRCTBL | Binary FITS table | src |

Table 6: data products and file types

Format of coadded images

The final calibrated, coadded images have a uniform pixel scale of 0.2 arcsec. The pixel units are fluxes relative to the flux corresponding to magnitude = 0. This means that the effective zeropoint is equal to 0 and the magnitude m corresponding to a pixel value f is:

$$m = -2.5 \log_{10} f.$$

Catalogue Columns

Table 7 lists the columns that are present in the single-band source lists provided in KiDS-ESO-DR1. A large number (27) of aperture fluxes, are provided to suit the needs of different users and allow interpolation to estimate e.g. aperture corrections. Only the columns for the smallest aperture (2 pixels, or 0.4 arcsec diameter) and the largest aperture (200 pixels, or 40 arcsec diameter) are listed in Table 7. Note: the label for the aperture of 28.5 pixels is FLUX_APER_28p5.

| Label | Format | Unit | Description |
|--------------|--------|-------|---|
| 2DPHOT | J | | Source classification (see section on star/galaxy separation) |
| X_IMAGE | E | pixel | Object position along x |
| Y_IMAGE | E | pixel | Object position along y |
| NUMBER | J | | Running object number |
| CLASS_STAR | E | | S-Extractor S/G classifier |
| FLAGS | J | | Extraction flags |
| IMAFLAGS_ISO | J | | FLAG-image flags OR'ed over the iso. profile |
| NIMAFLAG_ISO | J | | Number of flagged pixels entering IMAFLAGS_ISO |
| FLUX_RADIUS | E | pixel | Fraction-of-light radii |
| KRON_RADIUS | E | pixel | Kron apertures in units of A or B |

| Label | Format | Unit | Description |
|------------------|--------|--------------|---|
| FWHM_IMAGE | E | pixel | FWHM assuming a gaussian core |
| ISOAREA_IMAGE | J | pixel**2 | Isophotal area above Analysis threshold |
| ELLIPTICITY | E | | 1 - B_IMAGE/A_IMAGE |
| THETA_IMAGE | E | deg | Position angle (CCW/x) |
| MAG_AUTO | E | mag | Kron-like elliptical aperture magnitude |
| MAGERR_AUTO | E | mag | RMS error for AUTO magnitude |
| ALPHA_J2000 | D | deg | Right ascension of barycenter (J2000) |
| DELTA_J2000 | D | deg | Declination of barycenter (J2000) |
| FLUX_APER_2 | E | count | Flux vector within circular aperture of 2 pixels |
| ... | ... | ... | ... |
| FLUX_APER_200 | E | count | Flux vector within circular aperture of 200 pixels |
| FLUXERR_APER_2 | E | count | RMS error vector for flux within aperture of 2 pixels |
| ... | ... | ... | ... |
| FLUXERR_APER_200 | E | count | RMS error vector for flux within aperture of 2 pixels |
| MAG_ISO | E | mag | Isophotal magnitude |
| MAGERR_ISO | E | mag | RMS error for isophotal magnitude |
| MAG_ISOCOR | E | mag | Corrected isophotal magnitude |
| MAGERR_ISOCOR | E | mag | RMS error for corrected isophotal magnitude |
| MAG_BEST | E | mag | Best of MAG_AUTO and MAG_ISOCOR |
| MAGERR_BEST | E | mag | RMS error for MAG_BEST |
| BACKGROUND | E | count | Background at centroid position |
| THRESHOLD | E | count | Detection threshold above background |
| MU_THRESHOLD | E | arcsec**(-2) | Detection threshold above background |
| FLUX_MAX | E | count | Peak flux above background |
| MU_MAX | E | arcsec**(-2) | Peak surface brightness above background |
| ISOAREA_WORLD | E | deg**2 | Isophotal area above Analysis threshold |
| XMIN_IMAGE | J | pixel | Minimum x-coordinate among detected pixels |
| YMIN_IMAGE | J | pixel | Minimum y-coordinate among detected pixels |
| XMAX_IMAGE | J | pixel | Maximum x-coordinate among detected pixels |
| YMAX_IMAGE | J | pixel | Maximum y-coordinate among detected pixels |
| X_WORLD | D | deg | Barycenter position along world x axis |
| Y_WORLD | D | deg | Barycenter position along world y axis |
| XWIN_IMAGE | E | pixel | Windowed position estimate along x |
| YWIN_IMAGE | E | pixel | Windowed position estimate along y |
| X2_IMAGE | D | pixel**2 | Variance along x |
| Y2_IMAGE | D | pixel**2 | Variance along y |
| XY_IMAGE | D | pixel**2 | Covariance between x and y |
| X2_WORLD | E | deg**2 | Variance along X-WORLD (alpha) |
| Y2_WORLD | E | deg**2 | Variance along Y-WORLD (delta) |
| XY_WORLD | E | deg**2 | Covariance between X-WORLD and Y-WORLD |
| CXX_IMAGE | E | pixel**(-2) | Cxx object ellipse parameter |
| CYY_IMAGE | E | pixel**(-2) | Cyy object ellipse parameter |
| CXY_IMAGE | E | pixel**(-2) | Cxy object ellipse parameter |
| CXX_WORLD | E | deg**(-2) | Cxx object ellipse parameter (WORLD units) |
| CYY_WORLD | E | deg**(-2) | Cyy object ellipse parameter (WORLD units) |
| CXY_WORLD | E | deg**(-2) | Cxy object ellipse parameter (WORLD units) |
| A_IMAGE | D | pixel | Profile RMS along major axis |

| Label | Format | Unit | Description |
|----------------|--------|-------------|--|
| B_IMAGE | D | pixel | Profile RMS along minor axis |
| A_WORLD | E | deg | Profile RMS along major axis (WORLD units) |
| B_WORLD | E | deg | Profile RMS along minor axis (WORLD units) |
| THETA_WORLD | E | deg | Position angle (CCW/world-x) |
| THETA_J2000 | E | deg | Position angle (east of north) (J2000) |
| ELONGATION | E | deg | A_IMAGE/B_IMAGE |
| ERRX2_IMAGE | E | pixel**2 | Variance of position along x |
| ERRY2_IMAGE | E | pixel**2 | Variance of position along y |
| ERRXY_IMAGE | E | pixel**2 | Covariance of position between x and y |
| ERRX2_WORLD | E | deg**2 | Variance of position along X-WORLD (alpha) |
| ERRY2_WORLD | E | deg**2 | Variance of position along Y-WORLD (delta) |
| ERRXY_WORLD | E | deg**2 | Covariance of position X-WORLD/Y-WORLD |
| ERRCXX_IMAGE | E | pixel**(-2) | Cxx error ellipse parameter |
| ERRCYY_IMAGE | E | pixel**(-2) | Cyy error ellipse parameter |
| ERRCXY_IMAGE | E | pixel**(-2) | Cxy error ellipse parameter |
| ERRCXX_WORLD | E | deg**(-2) | Cxx error ellipse parameter (WORLD units) |
| ERRCYY_WORLD | E | deg**(-2) | Cyy error ellipse parameter (WORLD units) |
| ERRCXY_WORLD | E | deg**(-2) | Cxy error ellipse parameter (WORLD units) |
| ERRA_IMAGE | E | pixel | RMS position error along major axis |
| ERRB_IMAGE | E | pixel | RMS position error along minor axis |
| ERRA_WORLD | E | deg | World RMS position error along major axis |
| ERRB_WORLD | E | deg | World RMS position error along minor axis |
| ERRTHETA_IMAGE | E | deg | Error ellipse pos. angle (CCW/x) |
| ERRTHETA_WORLD | E | deg | Error ellipse pos. angle (CCW/world-x) |
| ERRTHETA_J2000 | E | deg | J2000 error ellipse pos. angle (east of north) |
| FWHM_WORLD | E | deg | FWHM assuming a gaussian core |
| ISO0 | J | pixel**2 | Isophotal area at level 0 |
| ISO1 | J | pixel**2 | Isophotal area at level 1 |
| ISO2 | J | pixel**2 | Isophotal area at level 2 |
| ISO3 | J | pixel**2 | Isophotal area at level 3 |
| ISO4 | J | pixel**2 | Isophotal area at level 4 |
| ISO5 | J | pixel**2 | Isophotal area at level 5 |
| ISO6 | J | pixel**2 | Isophotal area at level 6 |
| ISO7 | J | pixel**2 | Isophotal area at level 7 |
| SLID | K | | Source list ID |
| SID | K | | Source ID within the source list |
| HTM | K | | Hierarchical Triangular Mesh (level 25) |
| FLAG | K | | Not used |

Table 7: columns provided in the KiDS-ESO-DR1 single-band source lists

Acknowledgements

The following acknowledgment is valid at the moment of writing this document. For an up-to-date version, please visit the following webpage:

<http://kids.strw.leidenuniv.nl/DR1/acknowledgements.php>

Users of data from this release should cite “de Jong et al. (2013, ExA 35, 25)”.

Please use the following statement in your articles when using these data:

Based on data products from observations made with ESO Telescopes at the La Silla Paranal Observatory under programme IDs 177.A-3016, 177.A-3017 and 177.A-3018, and on data products produced by Target/OmegaCEN, INAF-OACN, INAF-OAPD and the KiDS production team, on behalf of the KiDS consortium. OmegaCEN and the KiDS production team acknowledge support by NOVA and NWO-M grants. Members of INAF-OAPD and INAF-OACN also acknowledge the support from the Department of Physics & Astronomy of the University of Padova, and of the Department of Physics of Univ. Federico II (Naples).